Rezoug A, Iqbal J, Tadjine M. Extended grey wolf optimization–based adaptive fast nonsingular terminal sliding mode control of a robotic manipulator. Proceedings of the Institution of Mechanical Engineers, Part I: Journal of Systems and Control Engineering. June 2022 Copyright © 2022 SAGE Publications. DOI: 10.1177/09596518221099768

Extended Grey wolf Optimization Based Adaptive Fast Nonsingular Terminal Sliding Mode Control of a Robotic Manipulator

Amar Rezoug[1], Jamshed Iqbal[2] and Mohamed Tadjine[3]

Abstract

This paper proposes a novel hybrid meta-heuristic technique based on Nonsingular Terminal Sliding Mode Controller (NTSMC), Time Delay Estimation (TDE) method, an Extended Grey Wolf Optimization (EGWO) algorithm and adaptive super twisting control law. The fast convergence is assured by NTSMC owing to its inherent nonlinear property and no prior knowledge of the robot dynamics is required due to TDE. The proposed EGWO algorithm determines an optimal approximation of the inertial matrix of the robot. Moreover, adaptive super twisting control based on the Lyapunov approach overcomes the disturbances and compensate the higher dynamics not achievable by the TDE method. Firstly, the Fast NTSMC (F-NTSMC) relying on TDE is designed and is combined with super twisting control for chattering attenuation. The constant gain matrix of the time delay is determined by the proposed EGWO algorithm. Secondly, an adaptive law based on Lyapunov stability theorem is designed for improving tracking performance in the presence of uncertainties and disturbances. The novelty of the proposed method lies in the adaptive law where the prior knowledge of parametric uncertainties and disturbances is not needed. Moreover, the constant gain matrix of TDE method is obtained using the proposed algorithm. The control method has been tested in simulation on a three Degrees of Freedom (DOF) robotic manipulator in trajectory tracking mode in the presence of control disturbances and uncertainties. The results obtained confirmed the effectiveness, robustness and the superior precision of the proposed control method compared to the classical ones.

Introduction

The advancements in robotics and automation have reshaped various processes in industry during last few decades [1-3]. Robotic manipulators are now an integral part of automation where their performance is relies on the associated control law [4]. Despite several research works reporting linear methods [5-7] as well as non-linear approaches [8-12] to control a robotic manipulator, it is still an open research problem in the scientific community. It is reported that modern control techniques based on nonlinear control laws offer superior performance compared to linear and classical approaches [13].

Owing to robustness against internal and external uncertainties and modelling inaccuracies, Sliding Mode Control (SMC) or its variants are prominent nonlinear approaches to address the control problem of a robotic manipulator [14,15]. Terminal SMC (TSMC) is a new control variant that is recently widely investigated. Nonsingular TSMC (NTSMC) is a discontinuous feedback control which has been applied to control second or higher order uncertain systems [16-20]. NTSMC can achieve a finite time convergence and can precisely maintain the system dynamics onto the selected nonlinear sliding manifold by means of a discontinuous control law. Moreover, NTSMC offers other distinguishing benefits compared to the conventional SMC including but not limited to; (i) Fast and relatively simple to implementation, (ii) Insensitivity to external disturbances and parametric uncertainties, (iii) Improved dynamic responses, (iv) Particularly useful for high precision control because of speed-up rate of convergence near the equilibrium point. However, NTSMC suffers from chattering problem [21]. The use of adaptive Higher Order SMC (HOSMC) is an alternative approach, which is able to attenuate the chatter phenomena while maintaining the adequate control performance.

Another control technique based on Time Delay Estimation (TDE) is considered as a simple and an effective control

[1]Laboratoire de Technologie Innovate, Ecole Nationale Superieure de Technologie, Diplomatic City, Dergana-Bordj El Kiffan, Algiers, Algeria
[2]Department of Computer Science and Technology, Faculty of Science and Engineering, University of Hull, HU6 7RX, UK
[3]Laboratoire de Commandes des Processus, Ecole Nationale Polytechnique Algiers, El Harrach, Algeria

Corresponding author:
Amar REZOUG, amar.rezoug@enst.dz

method when applied to nonlinear and complex systems. This is a preferred technique when the system dynamics is unknown. The basic idea of TDE is to estimate the unknown dynamics by using time-delayed information. The application of TDE to control a robotic maipulator is reported in [16,22,23].

The literature reports several combinations of TDE and NTSMC with and without adaptive HOSMC have been proposed for controlling robotic manipulators. One such work is reported in [17], where an experimental application was successfully realized for a real 3-Degrees Of Freedom (DOF) robotic manipulator. In [24] a continuous fractional-order NTSMC scheme based on TDE is presented with an application to a 2-DOF cable-driven manipulator. In [25], an approach based on fast NTSMC (F-NTSMC) and adaptive HOSMC was proposed in simulation for a 2-DOF manipulator in the presence of parametric uncertainties and external control disturbances. The chattering effect was eliminated with the assumption that model of the robot is available. Another research work relying on robot model is reported in [18], where an adaptive dual TSMC was proposed for controlling a rigid manipulator. Proportional Integral Derivative (PID) sliding manifold based SMC was considered in [26] which used function approximation technique based on Legendre polynomial to approximate the uncertainty factors online. An underwater manipulator was explored in this work to validate the proposed method. In [27], an inverse kinematics methodology based on adaptive super-twisting controller was developed to compensate the unknown uncertainty in the Jacobian matrix of a serial-link manipulator. The research work reported in [28] represented a robust hybrid fractional order proportional derivative SMC for a 2-DOF robotic manipulator based on Extended Grey Wolf Optimizer (EGWO).

A thorough review of literature revealed that most of the relevant reported works suffer from one or more of the following drawback(s):

(i) Chattering is removed by the use of saturation function. However, use of this method limits the robustness range to the saturation bound. Moreover the rapidity and accuracy get depreciated.
(ii) The gain in TDE-based control methods is obtained by trial and error approach, thus possibly limiting the precision and robustness of the reported methods [16]. Furthermore, TDE always involves a restricted magnitude of gain in a robotic manipulator because the stability criterion is closely related to the magnitude of the TDE-based control gains.
(iii) The control is based on the model of a robot. In real-world applications, it is not always possible to have a realistic model of a robot.
(iv) A linear sliding manifold is used, which limits the performance that can be achieved since all the systems are inherently nonlinear in nature.

On the other hand, meta-heuristic optimization methods have recently become an interesting multi-disciplinary research area [29]. The principle of these methods is inspired by the natural behaviour of animals [30]. One of the recently reported meta-heuristic algorithms is GWO, which mimics the behaviour of the leadership hierarchy and hunting mechanism of grey wolves in nature [31]. This method is used in the present work to optimize a constant diagonal matrix that replaces the inertial matrix of the manipulator's dynamics [32].

This research aims to propose a novel control method based on the combination of NTSMC, TDE, GWO and an adaptive HOSMC. NTSMC is used for ensuring precision and robustness while TDE method is utilized to estimate unknown dynamics of the robotic manipulator. GWO algorithm is used to estimate inertial diagonal matrix $\bar{M}$ termed as a gain in the present work. This is directly related to the magnitude of the inertial matrix of a robotic manipulator. However, it is not straight forward to determine the inertial matrix of a robotic manipulator and thus this problem is closely related to the practice aspect in real systems [16]. To the best of authors' knowledge, the matrix $\bar{M}$ in all the works reported to-date has been found by trial and error approach, which cannot guarantee the best performance that could be offered by these control methods. From this perspective, the primary novelty of the present research is to propose a method to obtain the matrix $\bar{M}$ by using a meta-heuristic technique. An adaptive super twisting control law based on Lyapunov stability condition is also proposed to deal with chattering phenomena. The use of TDE generates inevitable estimation errors that can further deteriorate the control performance, especially when the system dynamics varies quickly. This highlights the potential and need to use robust control methods that work with TDE to maintain adequate performance. The application of TDE requires a diagonal matrix that replaces the robot inertia matrix. Instead of determining this matrix by trial and error, an optimal matrix is found by the proposed EGWO approach. TDE usually acts as a basic structure without involving the system model and subsequently, a robust control law is applied to obtain a fast-dynamic response with high precision.

The contributions of the present research can be summarized below:

(1) A novel Extended Grey Wolf optimized Fast-NTSMC (EGF-NTSMC) technique is proposed by introducing a new EGWO to obtain inertial diagonal matrix $\bar{M}$ which previously was obtained by trial and error method.
(2) The newly proposed EGF-NTSMC is combined with an adaptive law to formulate a hybrid control scheme termed as Adaptive EGF-NTSMC (AEGF-NTSMC).
(3) The effectiveness of the proposed control schemes is demonstrated in trajectory tracking mode using a 3-DOF robotic manipulator (Figure 1) based on

comparative simulation results involving parametric uncertainties and control input disturbances.

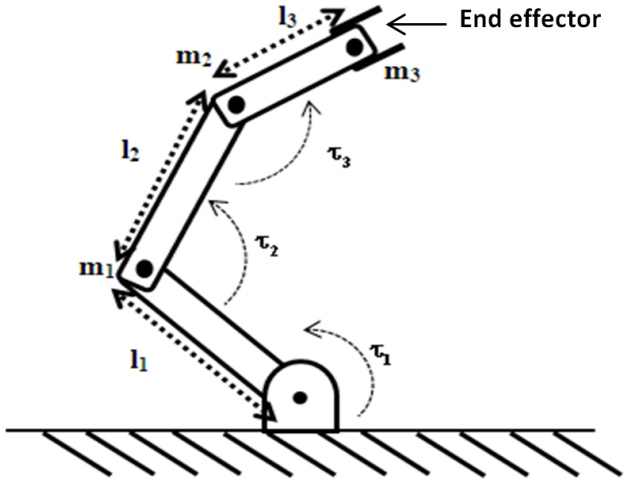

Figure 1. 3-DOF robotic manipulator, l_1, l_2, l_3 denote the link lengths, m_1, m_2, m_3 re
present the link masses, τ_1, τ_2, τ_3 are the control signals

The remaining of the paper is organized as follows: Section II presents the preliminary background, which includes the robot model and short description of the techniques and methods relevant to the present work. Section III and Section IV detail the design of the EGF-NTSMC and AEGF-NTSMC respectively. Simulation results are presented in Section V. Finally, Section VI concludes the paper.

II. Preliminaries

II.1. Robotic manipulator model [17,38]

The dynamic model of a n-DOF robotic manipulator is given as

$$M\left(q,\dot{q}\right)\ddot{q}+C\left(q,\dot{q}\right)\dot{q}+G\left(q\right)+F\left(q\right)+\tau_d=\tau \qquad (1)$$

where $M\left(q,\dot{q}\right)\in R^{n\times n}$ is the inertial matrix, $C\left(q,\dot{q}\right)\in R^{n\times n}$ is the vector of Centrifugal and Coriolis forces and $F\left(q,\dot{q}\right)\in R^{n\times 1}$ is the friction vector. $G\left(q\right)\in R^{n\times 1}$ is the vector of gravity terms, $q\in R^{n\times 1}$, $\dot{q}\in R^{n\times 1}$ and $\ddot{q}\in R^{n\times 1}$ are position, velocity and acceleration vectors respectively. $\tau\in R^{n\times 1}$ is the torque input vector and $\tau_d\in R^{n\times 1}$ are the unknown bounded disturbances. The following Property is verifiable [38] $M(q)-2C(q,\dot{q})$ sew-symmetric.

II.2. TDE

The main idea behind TDE is to estimate unknown dynamics and disturbances by using time-delayed information [12,17]. Re-writing the model (1) as

$$\bar{M}u+N\left(\ddot{q},\dot{q},q\right)=\tau \qquad (2)$$

where $\bar{M}$ is a diagonal constant matrix to be designed and adjusted through EGWO algorithm. And u is given as

$$u=\ddot{q}+\varepsilon \qquad (3)$$

where ε represents the mismatched modelling part and $N\left(\ddot{q},\dot{q},q\right)=\left[M\left(q,\dot{q}\right)-\bar{M}\right]\ddot{q}+C\left(q,\dot{q}\right)\dot{q}+G\left(q\right)+\tau_d$ represents the remaining lumped unknown dynamics of the close-loop control system. It is generally complex to accurately determine N. So, (2) is also taken as equivalent to

$$\bar{M}u+\tilde{N}\left(\ddot{q},\dot{q},q\right)=\tau \qquad (4)$$

where $\tilde{N}\left(\ddot{q},\dot{q},q\right)$ is the estimation of $N\left(\ddot{q},\dot{q},q\right)$ and can be obtained using TDE method as

$$\bar{M}\ddot{q}_{t-L}+N_{t-L}\left(\ddot{q},\dot{q},q\right)=\tau_{t-L} \qquad (5)$$

where L is sufficiently small time-delay to ensure that TDE functions correctly. L is usually chosen to be the sampling time [17]. If we take

$$N_{t-L}\left(\ddot{q},\dot{q},q\right)=\tilde{N}\left(\ddot{q},\dot{q},q\right) \qquad (6)$$

Using (5) and (6), equation (4) becomes

$$\bar{M}\left(u-\ddot{q}_{t-L}\right)+\tau_{t-L}=\tau \qquad (7)$$

II.3. TSMC

: SMC is a useful robust nonlinear technique to handle disturbances and uncertainties [14]. During the last decades, several variants of SMC have been proposed. NTSMC is one of these variants characterized by the nonlinearity of the sliding surface. The applications of TSMC and its variants to robotic manipulators have been thoroughly investigated in scientific literature [11, 16–18, 34–39]. TSMC has the key advantage to ensure finite time convergence as reported in [20, 25, 40]. Singularity problem of TSMC has been overcome by the so-called NTSMC method [17]. F-NTSMC has been investigated for a robotic manipulator in [37], where this approach offered fast convergence of the robot even if the system states are far from equilibrium. NTSMC based TDE has been discussed in [11, 12, 22, 23, 40]. Numerous sliding surfaces have been proposed in the literature [19,33,34] such as

$$S=\dot{e}+k_1e^{q/p} \qquad (8)$$

$$S=e+{k_1}^{-1}\dot{e}^{p/q} \qquad (9)$$

$$S=\dot{e}+{k_1}^{-1}|e|^{p/q}sign(e) \qquad (10)$$

$$S=e+{k_1}^{-1}|\dot{e}|^{p/q}sign(\dot{e}) \qquad (11)$$

For all these surfaces, $S=[s_1,\ldots,s_i,\ldots,s_n]^T\in R^n$ is the sliding surface, $k_1=diag[k_{11},\ldots,k_{1i},\ldots,k_{1n}]\in R^{n\times n}$ is a matrix composed of positive constants, p and q are positive odd integers with $p>q$. All previous TSMC

will terminate subject to satisfying the following sufficient condition:

$$S\dot{S} \leq -\rho(e,\dot{e})|S| \tag{12}$$

where $\rho(e,\dot{e}) \in R^+$
$\rho \neq 0$ must be a positive defined function. For each case of the stability analysis, $V = 1/2S^TS$ is used as a Lyapunov candidate function. ρ can take a constant positive value. The reach time of the sliding surface (i.e. when $t_r \neq 0$) of all surfaces is defined as $t_{r_i} \leq \|S(0)|/K_{w_{ii}}$.with $K_{w_{ii}} > 0$

For a robotic manipulator controlled with TDE-based approach, the control laws in case of (8) and (9) are respectively written as,

$$\tau = \bar{M}(\ddot{q}_d - \ddot{q}_{t-L} + k_1\gamma^{-1}\dot{e}e^{1-\gamma} + K_w sign\,(S)) + \tau_{t-L} \tag{13}$$

$$\tau = \bar{M}(\ddot{q}_d - \ddot{q}_{t-L} + (\gamma k_1)^{-1}\dot{e}^{2-\gamma} + K_w sign\,(S)) + \tau_{t-L} \tag{14}$$

where $\gamma = p/q$, and $1 < \gamma < 2$. K_w is a positive diagonal matrix.
The control law given in (13) leads to singularity if $e = 0$ and/or $\dot{e} = 0$, because $1 < \gamma < 2$.Moreover, $e^{1-\gamma} \notin R$ if $e < 0$. The control law expressed in (14) suffers from singularity if $\dot{e} < 0$, since $\dot{e}^{2-\gamma} \notin R$. The design of (13) an (14) designs are given in Appendix.

Once the Terminal Sliding Surface $S = 0$ is reached, the system dynamics of e is governed by

$$e = -k_1^{-1}|\dot{e}|^{p/q}sign(\dot{e})$$

Solving it for the finite time t_s from $e(t_r)$ to 0, we get

$$t_s = -\frac{1}{k_1}\int_{e(t_r)}^{0} e^{-q/p} = \frac{p}{k_1(p-q)}|e(t_r|^{(\gamma-1)}$$

II.4. Fast Nonsingular Terminal Sliding Mode Controller (F-NTSMC)

The sliding surface (S) for F-NTSMC of the robotic manipulator is chosen as

$$S = e + k_1|e|^{\zeta}sign\,(e) \;\; + k_2|\dot{e}|^{\gamma}sign\,(\dot{e}) \tag{15}$$

where k_1 and k_2 are real positive design diagonal matrices, e is the error vector i.e. $e = q_d - q$, and $\dot{e} = \dot{q}_d - \dot{q}$ is its time derivative, $sign$ is the signum function. The parameters γ and ζ must satisfy the condition $1 < \gamma < 2$ and $\zeta > \gamma$. The choice of this sliding manifold offers precision and robustness. The term $k_1|e|^{\zeta}sign\,(e)$ is added to handle the systems having states far from the equilibrium point by dominating the influence of the term $k_2|\dot{e}|^{\gamma}sign\,(\dot{e})$. On the other hand, when a state of the system is close to the equilibrium state, the term $k_2|\dot{e}|^{\gamma}sign\,(\dot{e})$ guarantees the convergence in a finite-time [25].

The time taken to travel from $e(t_r)$ to 0 is finite and is given in [35] as

$$t_s = -{k_2}^{\gamma^{-1}}\int_{e(t_r)}^{0}\frac{1}{(\eta + k_1\eta^{\zeta})^{\gamma^{-1}}}d\eta$$

In order to examine faster convergence performance of sliding surface (15) compared to that given in (10) and (11), we considered the following sliding modes: $S = \dot{e} + {k_1}^{-1}|e|^{p/q}sign(e) = 0$, $S = e + {k_1}^{-1}|\dot{e}|^{p/q}sign(\dot{e}) = 0$, and $S = e + k_1|e|^{\zeta}sign\,(e) \;\; + k_2|\dot{e}|^{\gamma}sign\,(\dot{e})$. For homogeneous comparison, sliding surfaces parameters are chosen as $\gamma = p/q = 7/5$, $k_1 = 1$. Since S_5 has a supplementary term $k_2|e|^{\zeta}sign(e)$, we can choose $\zeta(\zeta > \gamma)$ and k_2 as per our convenience. In this simulation, $k_2 = 1$ and $\zeta = 4$. Moreover, initial condition comprises of two values such as $e(0) = 5$ and $e(0) = -5$. Simulation results are given in Fig 2. It is clear from the Figure 2 that time convergence of Fast NTSMC using surface (15) is superior to that of NTSMC surfaces given by (10) or (11).

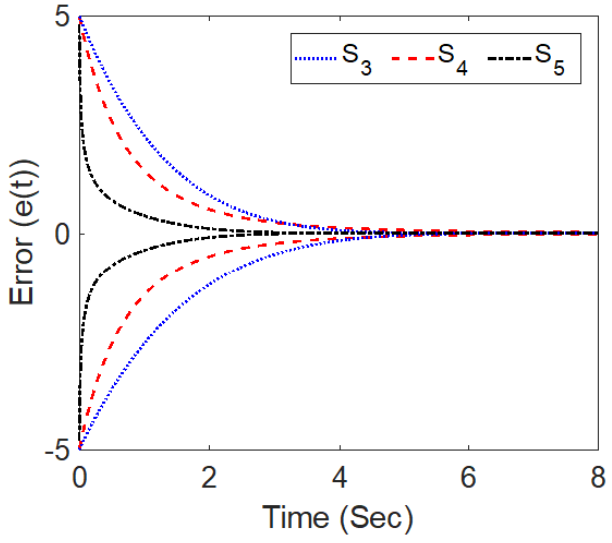

Figure 2. Comparison of terminal sliding surfaces (S_3 (10), S_4 (11) and S_5 (15))

The time derivative of (8) is

$$\dot{S} = \dot{e} + k_1\zeta|e|^{\zeta-1}\dot{e} \;\; + k_2\gamma|\dot{e}|^{\gamma-1}\ddot{e} \tag{16}$$

By equating (16) to zero (i.e. $\dot{S} = 0$) and replacing $\ddot{e} = \ddot{q}_d - \ddot{q}$, we obtain

$$[(1 + k_1\zeta|e|^{\zeta-1})\dot{e} \;\; + k_2\gamma|\dot{e}|^{\gamma-1}\,[\ddot{q}_d - \ddot{q}]] = 0$$

Combining with (3), we get

$$u = (k_2\gamma)^{-1}\left(1 + (k_1\zeta)\,|e|^{\zeta-1}\right)|\dot{e}|^{2-\gamma} sign\,(\dot{e}) + \ddot{q}_d + \Delta u \tag{17}$$

where Δu is the discontinuous control part, which is chosen as

$$\Delta u = -\frac{1}{2}\Gamma_1 |S|^{\frac{1}{2}} sign\,(S) - \Gamma_2 \int_0^t sign\,(S)\,dt - \eta sign\,(S) \tag{18}$$

where $\Gamma_1 = diag\,(\Gamma_{1ii}), \Gamma_2 = diag\,(\Gamma_{2ii})$ and $\eta = diag\,(\eta_{ii})$ are diagonal matrices with positive real values. The mismatched modelling term has been cancelled by the robust discontinuous part Δu. The term $-\eta sign\,(S)$ is called as compensation term. Substituting (17) into (7), the NTSMC law with TDE can be designed as

$$\tau = \bar{M}((k_2\gamma)^{-1}\left(1 + (k_1\zeta)\,|e|^{\zeta-1}\right)|\dot{e}|^{2-\gamma} sign\,(\dot{e}) + \ddot{q}_d + \Delta u - \ddot{q}_{t-L}) + \tau_{t-L} \tag{19}$$

The super twisting control law given in (19) involves a compensation term that improves robustness of the control. The mismatched modelling has been cancelled by the compensation term $-\eta sign\,(S)$. In addition, adaptive super twisting law has two effects; firstly, it can reduce the chattering phenomena and keeps the performances of the robot under control. Secondly, the combination of super twisting with the compensation term can potentially improve the control performance and maintain superior robustness. In (19), the gain matrix $\bar{M}$ is multiplied with all the sub-items of the controller which signifies its role. Thus, obtaining the value of $\bar{M}$ by trial and error results in a loss of precision. In order to solve this crucial problem, a meta-heuristic optimization method called EGWO is used which is presented in Section III.

III. Optimized Fast NTSMC (GF-NTSMC) and Extended GF-NTSMC (EGF-NTSMC):

The effect of $\bar{M}$ on the control performance and robustness is crucial as can be seen in (19). Optimization methods can be classified into two main categories. The first category is the optimization based on analytical methods. A well-known example of this category is the gradient descent algorithm, which suffers from a local minima problem. The second category employs the bio-inspired optimization methods. They are based on population coding and iterative search of the optimal value of a fitness function in this population. Owing to the random characteristics, these methods have less possibility for stagnation into local minima. The observer method is also a good alternative approach to design a control law for a robotic manipulator, however the tracking performance and robustness of these methods is a function of the related design parameters. The $\bar{M}$ matrix is optimized by using GWO and an EGWO method. These algorithms and the objective function are detailed below:

III.1. Grey Wolf Optimization (GWO)

GWO is an emerging optimization method inspired by wolves' natural hunting behavior and the social hierarchy of the grey wolves. The algorithm offers simplicity and fast convergence compared to other meta-heuristic algorithms [31]. The social hierarchy of wolves is structured in four sub-groups denoted respectively as $\alpha,\ \beta,\ \delta$ and ω. Alpha (α) is the leader of the pack group generally composed of one wolf or two wolves. This group is responsible for essential decisions/selections like hunting, place of sleeping, time to walk and so on. Beta (β) is the subordinate of the leader and their principal work is to assist α in accomplishment of their tasks. Delta (δ) occupies third position in the group in which the wolves are subordinates and assistants of β wolves. Rest of the wolves belong to the last category of the group named as omega (ω). The survival of wolves is essentially based on the quest for eating and to achieve this objective, a mission has to be organized with a high degree of accuracy. The mission includes encircling, hunting and then attacking a prey. The functionality of GWO algorithm can be summarized in three steps: (i) The given problem is mathematically formulated and required parameters are then initialized. (ii) A pack of grey wolves is randomly initialized in the search space domain. (iii) α, β and δ grey wolves lead the pack to search, pursue, and encircle a prey. When the prey is encircled by the grey wolves, the search finishes and attack begins. These steps are modelled mathematically and are detailed as follows: Wolves live by hunting and in order to realize the hunt, they follow two steps; the first step is exploration which involves search of a prey. Second phase is the exploitation, which consists of encircling, hunting and attacking the prey. Parameters $\vec{A}$ and $\vec{C}$ in (20-21) define the exploration and exploitation behaviors. These parameters are obtained by the combination of the parameter $\vec{a}$ and the random numbers r_1 and r_2 as

$$\vec{A} = 2r_1\vec{a} - \vec{a} \tag{20}$$

$$\vec{C} = 2r_2 \tag{21}$$

where r_1 and r_2 lie in the range [0, 1].

Parameter $\vec{a}$ is defined to be linearly decreasing from 2 to 0 using the following relationship

$$\vec{a}\ = 2\left(1 - \frac{actual\_iteration}{\max\_iteration}\right)$$

Exploration: This task becomes active when $\mid A \mid > 1$. $\vec{C}$ plays the role of stimulating the algorithm in the event of

stagnation into a local minima.

Exploitation: This step is initialized when $\mid A \mid < 1$. It is further composed of encircling, hunting and attacking the prey as detailed below:
Encircling: The encircling behavior can be modelled with (22-23)

$$\vec{D} = \left| \vec{C}\vec{X}_p\left(t\right) - \vec{X}\left(t\right) \right| \tag{22}$$

$$\vec{X}\left(t+1\right) = \vec{X}_p\left(t\right) - \vec{A}\vec{D} \tag{23}$$

where t indicates the current iteration, $\vec{X}$ is the position vector of the grey wolf, $\overrightarrow{X_p}\left(t\right)$ represents the prey position vector.

Hunting: This natural behavior is modelled mathematically by (24)

$$\vec{X}\left(t+1\right) = \frac{\vec{X}_1 + \vec{X}_2 + \vec{X}_3}{3} \tag{24}$$

where $\vec{X}$ is the position of the victim. $\vec{X}_1$, $\vec{X}_2$ and $\vec{X}_3$ are the position vectors of the α, β and δ wolves respectively. When a prey is found, the iteration begins. Thereafter, the α, β and δ wolves would lead the ω wolves to pursue and eventually encircle the prey. Three coefficients each for $\vec{C}$ and $\vec{D}$ represent the encircling behavior:

$$\vec{D}_\alpha = \left| \vec{C}_1\vec{X}_\alpha\left(t\right) - \vec{X} \right|, \vec{D}_\beta = \left| \vec{C}_2\vec{X}_\beta\left(t\right) - \vec{X} \right|$$
$$\vec{D}_\delta = \left| \vec{C}_3\vec{X}_\delta\left(t\right) - \vec{X} \right|, \vec{X}_1 = \vec{X}_\alpha\left(t\right) - \vec{A}_1\vec{D}_\alpha$$
$$\vec{X}_2 = \vec{X}_\beta\left(t\right) - \vec{A}_2\vec{D}_\beta, \vec{X}_3 = \vec{X}_\delta\left(t\right) - \vec{A}_3\vec{D}_\delta \tag{25}$$

Attacking prey: After encircling the prey, the grey wolves start to attack. Mathematically, this behaviour is modelled by the $\vec{A}$ values, thus if $|A| < 1$ (20), $\vec{A}$ gets decreased with the increase in $\vec{a}$.

III.2. Extended Grey Wolf Optimizer (EGWO)

In order to improve the position of the preys (24) so as to consequently improve the hunting behavior, an EGWO is proposed. In the start of the search, all wolves have the same importance. With the progression of iterations, $\vec{X}_1$ will have more and more importance knowing that he is the leader of all the other wolves. Meanwhile, $\vec{X}_3$ will carry progressively less importance. Following this concept, the role of αs becomes more important as the prey is approached. In order to mathematically formulate this behaviour, the position of the prey is re-estimated using (26)

$$\vec{X}\left(t+1\right) = \frac{l_1\vec{X}_1 + l_2\vec{X}_2 + l_3\vec{X}_3}{3} \tag{26}$$

where $l_1 = 1 + \Delta\left(\frac{n}{N}\right)$, $l_2 = 1$ and $l_3 = 1 - \Delta\left(\frac{n}{N}\right)$. $0 < \Delta < 1$, n is the actual iteration, N is the maximum number of iterations. We can notice that with each iteration, the value of l_1 increases, while the value of l_3 decreases.

In order to verify the effectiveness of the proposed EGWO, it is tested under 10 benchmark fitness functions given in Table 1 and Table 2. For the sake of fair performance comparison between GWO and EGWO, we have used the same number of iterations, dimension (D) and agents which are: iterations=1000, D= 30, and agents=30.

The results obtained after 30 independent runs are listed in Table 3 in case of the unimodal benchmark functions and in Table 4 for the multimodal benchmark functions. Following the quantitative performance comparison between GWO and EGWO, the best, mean and worst values of the benchmark fitness functions are presented. Moreover, the standard deviation is also shown. The values close to the optimums (global minimal) are represented in bold face. Simulation results demonstrated the superiority of the proposed EGWO to provide a solution closer to the valid optimum value.

III.3. Objective function

The objective function is a special case of a generalized function written in the form of:

$$J = \int_0^t t^\iota e^\kappa dt$$

where e is the trajectory tracking error, ι and κ are both integers whose values are respectively taken between 0-1 and 1-2. All combinations are possible. If $\iota = 0$ and $\kappa = 1$, we have the conventional Integral of Absolute Error (IAE) while the values $\iota = 0$ and $\kappa = 2$ lead to Integral of Absolut error (ISE). IAE and ISE give equal importance to all the errors corresponding to initial time and final time regardless of the state of the control system. Therefore, optimizing the control response using these finesses functions may result in getting the responses with relatively small overshoot but long stabilization time or vice versa [23]. In order to deal with this problem, the Integral Time Absolute Error (ITAE) ($\iota = 1$ and $\kappa = 1$) and Integral Time Square Error (ITSE) ($\iota = 1$ and $\kappa = 2$) are proposed. Both of these functions are based on time weights of the error such that the error values associated with higher time range are significantly considered in our case. In order to find the best $\bar{M}$, the GWO algorithm is used to minimize the following objective function (integral-of-error-squared over time)

$$IE2T = \int_0^t te^2 dt \tag{27}$$

This objective function can ensure precision and robustness of the optimized parameters in the global control law [35].

Theorem 1: If F-NTSMC surface is set as given in (8), then the states of the system defined in (1) converge to the

Table 1. Unimodal benchmark fitness functions

Function	Range	f_{min}
$f_1(x) = \sum_{i=1}^{n} x_i^2$	[-100,100]	0
$f_2(x) = \sum_{i=1}^{n} \lvert x_i \rvert + \prod_{i=1}^{n} \lvert x_i \rvert$	[-10,10]	0
$f_3(x) = \sum_{i=1}^{n} \left(\sum_{j-1}^{i} x_j \right)^2$	[-100,100]	0
$f_4(x) = max_i \{ \lvert x_i \rvert ,\ 1 \leq i \leq n \}$	[-100,100]	0
$f_5(x) = \sum_{i=1}^{n-1} \left[100 \left(x_{i+1} - x_i^2 \right)^2 + (x_i - 1)^2 \right]$	[-30,30]	0
$f_6(x) = \sum_{i=1}^{n} (x_i + 0.5)^2$	[-100,100]	0
$f_7(x) = \sum_{i=1}^{n} i x_i^4 + random[0,1)$	[-1.28,1.28]	0

Table 2. Multimodal benchmark fitness functions

Function	Range	f_{min}
$f_8(x) = \sum_{i=1}^{n} -x_i \sin(\sqrt{\lvert x_i \rvert})$	[-500,500]	-418.9829 × 5
$f_9(x) = \sum_{i=1}^{n} \left[x_i^2 - 10\cos(2\pi x_i) + 10 \right]$	[-5.12,5.12]	0
$f_{10}(x) = -20\exp\left(-0.2\sqrt{\frac{1}{n}\sum_{i=1}^{n} x_i^2} \right) - exp\left(\sum_{i=1}^{n} \cos(2\pi x_i) \right) + 20 + e$	[-32,32]	0

Table 3. Unimodal benchmark functions' results

Function	Algorithm	Statistical results			
		Best	Mean	Worst	St. Dev
$f_1(x)$	GWO	3.7837e-61	3.9639e-59	5.0973e-58	2.8530e+03
	EGWO	**1.3777e-64**	1.3592e-61	2.8334e-60	2.6746e+03
$f_2(x)$	GWO	5.3292e-36	9.6229e-35	5.1713e-34	8.0499e+06
	EGWO	**1.0565e-37**	9.2196e-37	2.6423e-36	2.3108e+07
$f_3(x)$	GWO	4.6007e-21	3.6962e-17	5.8420e-16	61.5379
	EGWO	**1.5049e-23**	8.9245e-18	8.9531e-17	64.4167
$f_4(x)$	GWO	1.4308e-16	3.8166e-14	5.0953e-13	7.8262
	EGWO	**5.3970e-17**	4.2837e-15	2.5536e-14	7.1891
$f_5(x)$	GWO	25.9619	26.9179	28.7173	8.7346e+06
	EGWO	**25.2165**	26.9682	28.5399	8.6104e+06
$f_6(x)$	GWO	1.3040e-05	0.2462	0.7443	0.6046
	EGWO	**1.1218e-05**	0.2739	0.7527	0.6490
$f_7(x)$	GWO	1.8207e-04	9.0674e-04	0.0024	3.3471
	EGWO	**1.7052e-04**	8.4499e-04	0.0018	3.5025

Table 4. Multimodal benchmark functions' results

Function	Algorithm	Statistical results			
		Best	Mean	Worst	St. Dev
$f_8(x)$	GWO	-7.1265e+03	-5.9646e+03	-4.3495e+03	608.6663
	EGWO	**-7.1744e+03**	-6.1359e+03	-4.4238e+03	522.8577
$f_9(x)$	GWO	0	0.6490	6.1150	44.3691
	EGWO	**0**	0.2819	5.0300	44.3032
$f_{10}(x)$	GWO	1.5099e-14	1.5928e-14	2.2204e-14	2.1067
	EGWO	**7.9936e-15**	1.5099e-14	2.2204e-14	1.9870

sliding surface in a finite time. The control law can be written as follows:

$$\tau = \bar{M}^*((k_2\gamma)^{-1}\left[1 + (k_1\zeta)\left|e\right|^{\zeta-1})|\dot{e}|^{2-\gamma} sign\left(\dot{e}\right) + \ddot{q}_d + \Delta u - \ddot{q}_{t-L}\right] + \tau_{t-L} \quad (28)$$

The EGF-NTSMC law bears the same structure as that of NTSMC, however here the matrix $\bar{M}^*$ is computed through the EGWO algorithm. In this case, compared with NTSMC, the expected results become very consistent. However, the control law can be further improved by introducing an adaptive approach based on Lyapunov stability formulation discussed in Section IV.

IV. Adaptive Optimized Fast –NTSMC (AEGF-NTSMC):

The control of the robotic manipulator using EGF-NTSMC is not sufficient particularly in case of trajectory tracking in the presence of uncertainties and disturbances. Therefore, an adaptive control based on Lyapunov stability analysis is proposed in this section.

Theorem 2: The system given in (1) and rewritten as in (4) is controlled by the following law in finite time:

$$\tau = \bar{M}^*((k_2\gamma)^{-1}\left[1+(k_1\zeta)\left|e\right|^{\zeta-1})|\dot{e}|^{2-\gamma}\right. \\ \left. sign\left(\dot{e}\right)+\ddot{q}_d+\Delta u-\ddot{q}_{t-L}\right]+\tau_{t-L} \tag{29}$$

where Δu is given by (18) and

$$\left.\begin{array}{l}\dot{\Gamma}_1=\frac{1}{2}\delta_{\Gamma_1}S^T\varphi(\dot{e})|S|^{\frac{1}{2}}sign(S)\\ \dot{\Gamma}_2=\delta_{\Gamma_2}S^T\varphi(\dot{e})\int sign(S)dt\end{array}\right\} \tag{30}$$

with $\varphi\left(\dot{e}\right)=k\gamma|\dot{e}|^{\gamma-1}$

Remark 1: The adaptive law (30) gives the time derivative of the super twisting parameters. $\dot{\Gamma}_1$ and $\dot{\Gamma}_2$ are monotonous functions which confirm the positivity condition of the super twisting parameters. For the convergence time tr, S will be equal to zero (i.e $S\left(tr\right)\ =0$) so, the values of $\dot{\Gamma}_1$ and $\dot{\Gamma}_2$ will have upper bounds.

Remark 2: The difference between the three controllers is mentioned here: In (19), matrix $\bar{M}$ must be found by the user using trial and error. In case of (28), $\bar{M}$ has been replaced by $\bar{M}^*$, which is obtained using GWO. Moreover, in case of (29), an adaptive super twisting-based controller is proposed in addition to the use of $\bar{M}^*$.

Proof: Consider the Lyapunov candidate function

$$V=\frac{1}{2}S^TS+\frac{1}{2\delta_{\Gamma_1}}(\Gamma_1-{\Gamma_1}^*)^2+\frac{1}{2\delta_{\Gamma_2}}(\Gamma_2-{\Gamma_2}^*)^2 \tag{31}$$

where δ_{Γ_1} and δ_{Γ_2} are positive real constants. ${\Gamma_1}^*$and ${\Gamma_2}^*$are optimal positive values of Γ_1 and Γ_2 respectively. Parameters ${\Gamma_1}^*$ and ${\Gamma_2}^*$ are used in the stability analysis, however, they do not appear in the final stability condition or in the control law, so the knowledge of their values is not necessary.

The time derivative of the Lyapunov function yields

$$\dot{V}=S^T\dot{S}+\frac{1}{\delta_{\Gamma_1}}(\Gamma_1-\Gamma_1^*)\dot{\Gamma}_1+\frac{1}{\delta_{\Gamma_2}}(\Gamma_2-\Gamma_2^*)\dot{\Gamma}_2 \tag{32}$$

From (3), we have

$$\ddot{e}=\ddot{q}_d-\ddot{q}=\ddot{q}_d-(u-\varepsilon) \tag{33}$$

Substituting (33) in (16) and then using (17), we get

$$\dot{S}=\varphi\left(\dot{e}\right)\left(\Delta u+\varepsilon\right) \tag{34}$$

Using (34), (32) can be re-written as

$$\dot{V}=S^T\varphi(\dot{e})\Big(\Delta u+\epsilon\Big)+\frac{1}{\delta_{\Gamma_1}}(\Gamma_1-\Gamma_1^*)\dot{\Gamma}_1+\frac{1}{\delta_{\Gamma_2}}(\Gamma_2-\Gamma_2^*)\dot{\Gamma}_2 \tag{35}$$

Now, involving (18) into $\dot{V}$ and adding and subtracting $\frac{1}{2}{\Gamma_1}^*|S|^{\frac{1}{2}}sign\left(S\right)$ and ${\Gamma_2}^*\int sign\left(S\right)dt$ yields

$$\begin{aligned}\dot{V}=&S^T\varphi(\dot{e})\Big[-\frac{1}{2}(\Gamma_1-\Gamma_1^*)|S|^{\frac{1}{2}}sign(S)\\&-\frac{1}{2}\Gamma_1^*|S|^{\frac{1}{2}}sign(S)-(\Gamma_2-\Gamma_2^*)\int_0^t sign(S)dt\\&-\Gamma_2^*\int_0^t sign(S)dt-\eta sign(S)+\epsilon\Big]+\frac{1}{\delta_{\Gamma_1}}(\Gamma_1-\Gamma_1^*)\dot{\Gamma}_1\\&+\frac{1}{\delta_{\Gamma_2}}(\Gamma_2-\Gamma_2^*)\dot{\Gamma}_2\end{aligned} \tag{36}$$

Equation (36) can be re-arranged as

$$\begin{aligned}\dot{V}=&S^T\varphi(\dot{e})\{-\eta sign(S)+\epsilon\}+\\&\Big[-\frac{1}{2}S^T\varphi(\dot{e})|S|^{\frac{1}{2}}sign(S)+\frac{1}{\delta_{\Gamma_1}}\dot{\Gamma}_1\Big]\Gamma_1\\&+\Big[-S^T\varphi(\dot{e})\int_0^t sign(S)dt+\frac{1}{\delta_{\Gamma_2}}\dot{\Gamma}_2\Big]\Gamma_2\\&-\frac{1}{2}\Gamma_1^*S^T\varphi(\dot{e})|S|^{\frac{1}{2}}sign(S)-\Gamma_2^*S^T\varphi(\dot{e})\int_0^t sign(S)dt\end{aligned} \tag{37}$$

Taking into account (30), (38) becomes

$$\dot{V}=S^T\varphi\left(\dot{e}\right)\{-\eta sign\left(S\right)\ +\varepsilon\}-\\ \frac{1}{2}{\Gamma_1}^*S^T\varphi\left(\dot{e}\right)|S|^{\frac{1}{2}}sign\left(S\right)-{\Gamma_2}^*S^T\varphi\left(\dot{e}\right)\int sign\left(S\right)dt$$

Since the second and third terms are negative, so the stability is verified iff

$$S^T\varphi\left(\dot{e}\right)\left(-\eta sign\left(S\right)\ +\varepsilon\right)\leq 0$$

Since $\varphi\left(\dot{e}\right)\geq 0$, we can guarantee that $\dot{V}\leq 0$ iff

$$\varepsilon\leq\eta \tag{38}$$

On the other hand, $\varepsilon=\bar{M}^{-1}\left(N\left(\ddot{q},\dot{q},q\right)-\tilde{N}\left(\ddot{q},\dot{q},q\right)\right)$ which results in

$$\left(N\left(\ddot{q},\dot{q},q\right)-\tilde{N}\left(\ddot{q},\dot{q},q\right)\right)\leq\bar{M}^*\eta \tag{39}$$

Remark 3: Inequality (39) confirms that the stability is strongly related to the accuracy of the estimation of

$N(\ddot{q}, \dot{q}, q)$. It is pertinent to mention here that the estimation of the $N(\ddot{q}, \dot{q}, q)$ is a strong function of sampling time involved. The objective of TDE is to estimate N given the value of $(\tilde{N})$ such that the estimation error is minimal. Ideally, the error should be zero which essentially implies that a good estimation stability is guaranteed.

The criteria that help to decide sampling time for the TDE algorithm is the time required to make the model operational and to perform control calculations as well as their interactions at each iteration. The sampling time is also related to the specification of the processor used. In case, the sampling time (period time) is insufficient due to the rapid change in the system dynamics, the proposed robust controller overcomes this issue.

Remark 4: The condition given in (38) can also be verified in case ε has a superior bound. Interested readers are referred to [17].

Remark 5: In order to guarantee that $\bar{M}$ does not affect the convergence proof, the search space of $\bar{M}$ is chosen intentionally to be positive. In addition, we can see the advantage of this method from the stability perspective that the final convergence condition is only dependent on $\bar{M}$. This implies that the value of $\bar{M}$ is determined prior to applying the adaptive control law.

V. Simulation Results and Discussions

The effectiveness of the proposed control strategies is demonstrated by conducting series of simulations on a 3-DOF rigid-link planar robotic manipulator in MATLAB/Simulink 2021 environment running on HP Pavilion laptop with 1.3Ghz CPU, AMD E1-6010APU and AMD Radeon R2 Graphics and 4.00 GB RAM. The physical parameters of the robotic manipulator shown in Fig 2 are listed in Table 5. The derived dynamic model of the manipulator is given in (40). Simulations have been carried out using two nonlinear trajectories given in (41) and (42). The simulation time and sampling time are 10 sec and g=9.8 m/sec^2 respectively. Selected control parameters for our proposed controller are summarized in Table 6.

$$\begin{bmatrix} M_{11} & M_{12} & M_{13} \\ M_{21} & M_{22} & M_{23} \\ M_{31} & M_{32} & M_{33} \end{bmatrix} \begin{bmatrix} \ddot{q}_1 \\ \ddot{q}_2 \\ \ddot{q}_3 \end{bmatrix} + l_1 l_1 sin(q_2) \begin{bmatrix} C_{11} & C_{12} & C_{13} \\ C_{21} & C_{22} & C_{23} \\ C_{31} & C_{32} & C_{33} \end{bmatrix} \begin{bmatrix} \dot{q}_1 \\ \dot{q}_2 \\ \dot{q}_3 \end{bmatrix} + \begin{bmatrix} 0 \\ 0 \\ -m_3 g \end{bmatrix} + \begin{bmatrix} 0.2sign(S_1) \\ 0.2sign(S_2) \\ 0.2sign(S_3) \end{bmatrix} = \tau + \tau_d \quad (40)$$

where

$M_{11} = l_1^2\left(\frac{m_1}{3} + m_2 + m_3\right) + l_1 l_2 (m_2 + 2m_3)\cos(q_2) + l_2^2\left(\frac{m_2}{3} + m_3\right)$

Table 5. Robot parameters

Parameter	Unit	Link 1	Link 2	Link 3
m	Kilogram (Kg)	1	0.8	0.5
l	Meter (m)	1	0.8	0.6

$M_{12} = M_{21} = -l_1 l_2\left(\frac{m_2}{2} + m_3\right)\cos(q_2) - l_2^2\left(\frac{m_2}{3} + m_3\right)$
$M_{13} = M_{23} = M_{31} = M_{32} = 0$
$M_{22} = -l_2^2\left(\frac{m_2}{2} + m_3\right)$
$M_{33} = m_3$
$C_{11} = -\dot{q}_2(m_2 + 2m_3)$
$C_{12} = C_{22} = -\dot{q}_2\left(\frac{m_2}{2} + m_3\right)$
$C_{13} = C_{22} = C_{23} = C_{31} = C_{32} = C_{33} = 0$

The numerical simulation involves the sampling L, which is the time period to execute one control task. This includes calculation of the model, the control law and transmission and reception of information to/from the system. So, L corresponds to time involved in one iteration of a closed-loop task. Various control techniques under discussion (F-NTSMC, GF-NTSMC, EGF-NTSMC and AEGF-NTSMC) are compared in simulation in terms of performance achieved by each of these. Results consist of illustrations of joints' responses, errors in angular positions, sliding variables, command signals, phase portraits and adaptive gains. NFTSMC parameters are chosen by trial and error. For GF-NTSMC and EGF-NTSMC, $\bar{M}^*$matrix parameters are obtained through GWO and EGWO algorithm respectively. The obtained values in case of GWO are $\bar{M}^* = diag(m_{ii}) = diag\ (0.19377,\ 0.0419184,\ 0.55882)\ \mathrm{kgm}^2$ and in case of EGF-NTSMC is $\bar{M}^* = diag(m_{ii}) = diag\ (0.38808,\ 0.06075,\ 0.83928)\ \mathrm{kgm}^2$. The $\bar{M}$ matrix parameters obtained by trial and error are: $\bar{M} = diag(m_{ii}) = diag\ (0.4,\ 0.2,\ 0.1)\ \mathrm{kgm}^2$ In AEGF-NTSMC, the super twisting parameters such as Γ_1 and Γ_2 are computed using (30).

The control task under discussion involves moving three links of the manipulator from an initial position $(q_{d1}(0), q_{d2}(0), q_{d3}(0)) = (0, 0, 0)\ rad$ to the trajectory given by

$$\left.\begin{array}{l} q_{d1}(t) = 1 + \sin(\pi t) \\ q_{d2}(t) = 1 + \sin(\pi t) \\ q_{d3}(t) = 1 + \sin(\pi t) \end{array}\right\} \quad (41)$$

In case of F-NTSMC, GF-NTSMC and EGF-NTSMC, the values of $diag(\Gamma_{11}(t), \Gamma_{12}(t), \Gamma_{13}(t)) = (100, 80, 100)$,$diag(\Gamma_{21}(t), \Gamma_{22}(t), \Gamma_{23}(t)) = (1, 1, 1)$ are considered. For AEGF-NTSMC, same parameters are used, however we started with the initial values of $diag(\Gamma_{11}(0), \Gamma_{12}(0), \Gamma_{13}(0)) = (0, 0, 0)$ and $diag(\Gamma_{21}(0), \Gamma_{22}(0), \Gamma_{23}(0)) = (0, 0, 0)$. Later, these values are updated based on the law given in (30).

Figures 3-5 depict an example of sinusoidal control task. It is evident that the input of AEGF-NTSMC varies smoothly showing very minimal fluctuations caused by the

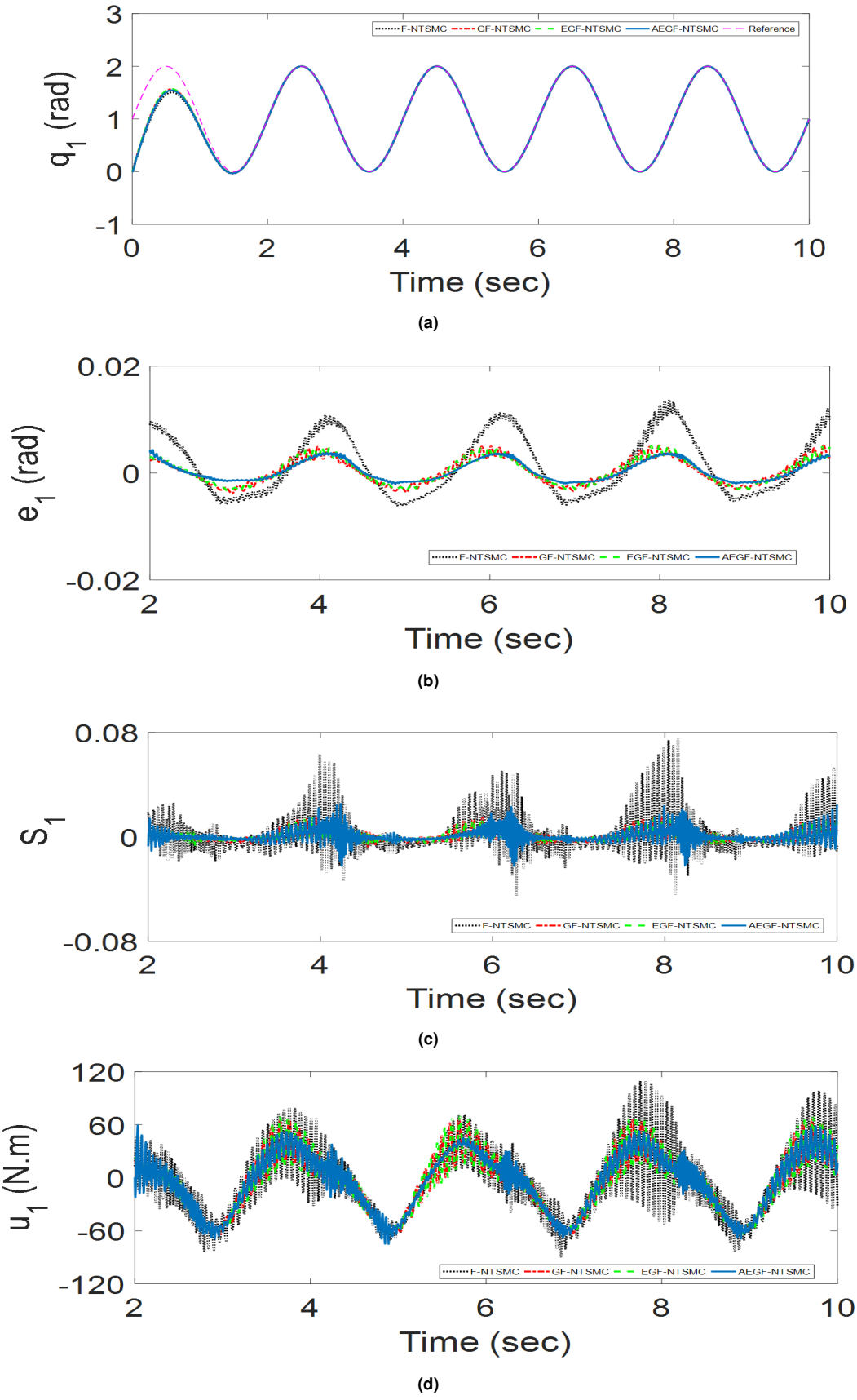

Figure 3. Position tracking performance of joint 1: (a) Joint response (b) Angular error (c) Sliding surface (d) Control input

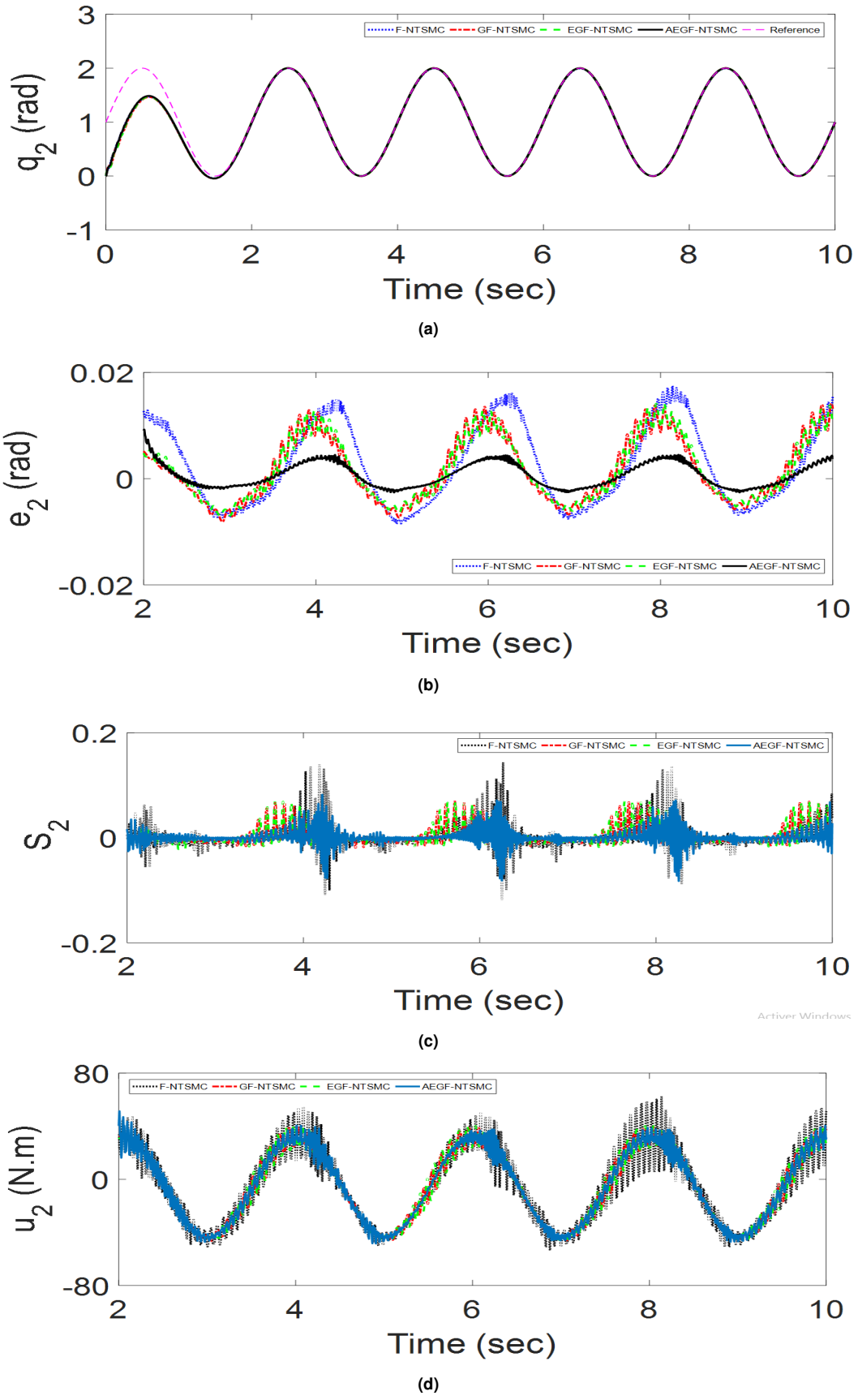

Figure 4. Position tracking performance of joint 2: (a) Joint response (b) Angular error (c) Sliding surface (d) Control input

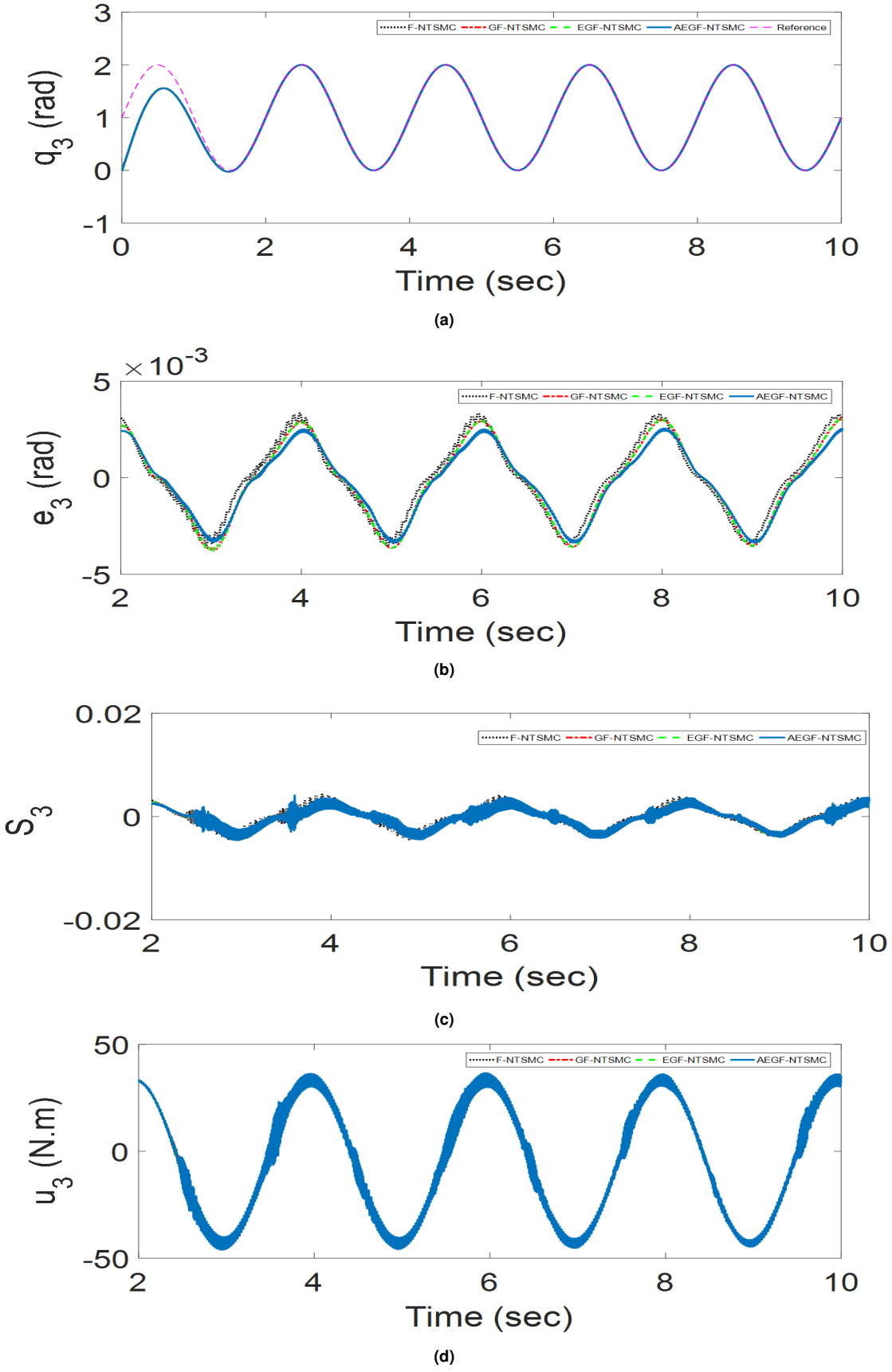

Figure 5. Position tracking performance of joint 3: (a) Joint response (b) Angular error (c) Sliding surface (d) Control input

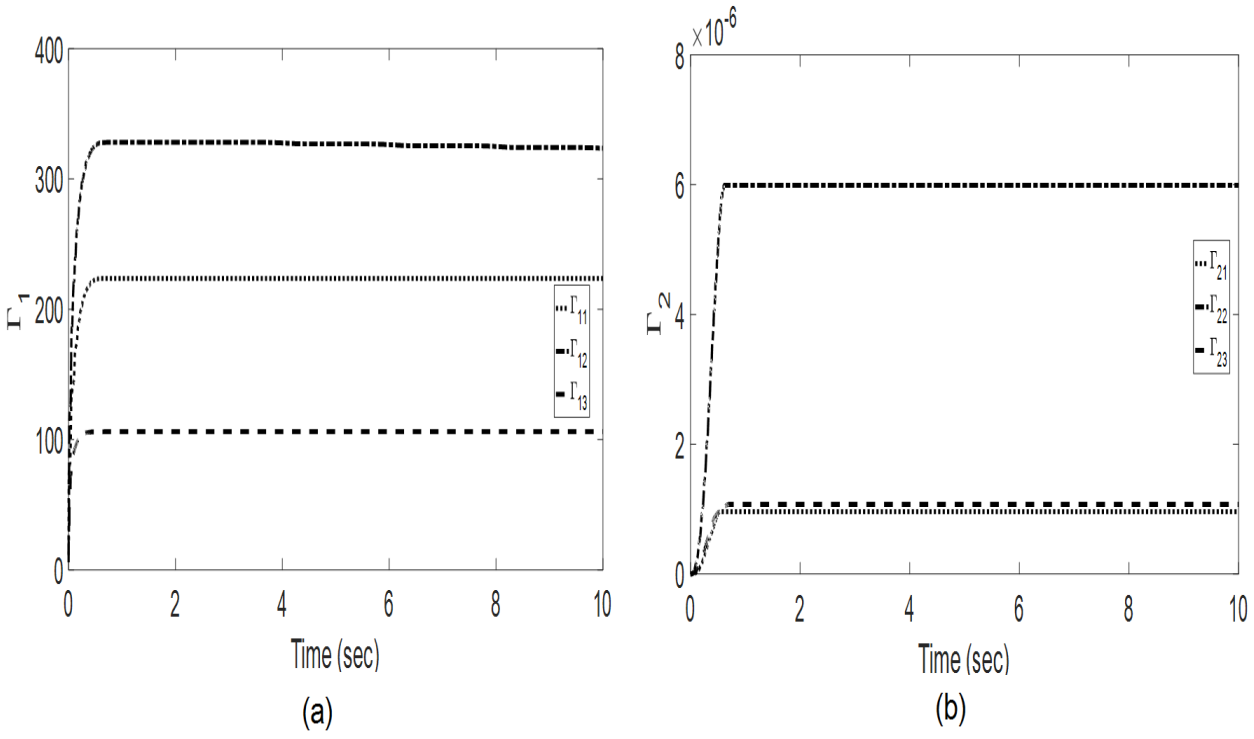

Figure 6. Adaptive gains of the AEGF-NTSMC (a) Alpha (b) Beta

actuator's efforts. These oscillations are decreased from link 1 to link 3 which is justified by the fact that link 1 makes more effort compared to link 2. The same holds true in case of link 2 and link 3. Therefore, by using EGF-NTSMC and AEGF-NTSMC, the three-joint robotic manipulator achieves the desired performance with good tracking precision. It can also be remarked that the precision of the AEGF-NTSMC is better (i.e. maximal errors for joints are $|e_{max1}| \leq 0.0058\ rad$, $|e_{max2}| \leq 0.0062\ rad$, $|e_{max3}| \leq 0.0034\ rad$) compared with others controllers under discussion. Indeed, F-NTSMC presents some imprecision particularly in case of link 1. The plots of sliding variables in different cases prove significant reduction in the chattering effects for all the controllers, owing to the role of the super twisting. The reduction is more in AEGF-NTSMC because of the adaptive action. All the controllers demonstrated robustness as indicated by the sliding surfaces. Adaptive parameters are shown in Fig. 6, which demonstrates that all the parameters converge to constant values indicating that the parameters are adaptively tuned until the sliding variables converge to the equilibrium. The fast convergence to zero phase portraits shown in Fig. 7 confirm the superiority of AEGF-NTSMC compared with F-NTSMC, GF-NTSMC and EGF-NTSMC. The control input signals in case of GF-NTSMC, EGF-NTSMC and AEGF-NTSMC show minimal chattering compared with F-NTSMC particularly corresponding to link 1 and link 2. For link 3, same chattering level is demonstrated by the three controllers which is justified by the fact that the control of link 3 does not require any supplementary effort to maintain the joint in the desired angle.

Table 6. Parameters for the proposed control strategies

Parameter	Value for Link 1-3
γ	1.6667
ζ	1.8333
k_1	1
k_2	1
η	1

Robustness verification

For robustness verification, the robotic manipulator is subjected to trajectory tracking mode involving parameter variations and external disturbances. The robot's joints are initialized to the position of $(q_{d1}(0), q_{d2}(0), q_{d3}(0)) = (0, 0, 0)\ rad$. The joints are then commanded to track the desired trajectory given by (42). The robustness is tested by modifying the link lengths and masses which are supposed to be uncertain. Hence, an additive variance of 10% for the joint one, 20% for joint 2 and 100% for joint 3 from their nominal values are considered as given in (43). The length of link 3 is assumed to have an additive uncertainty of 20% from its nominal value as indicated in (44). The choice to increase

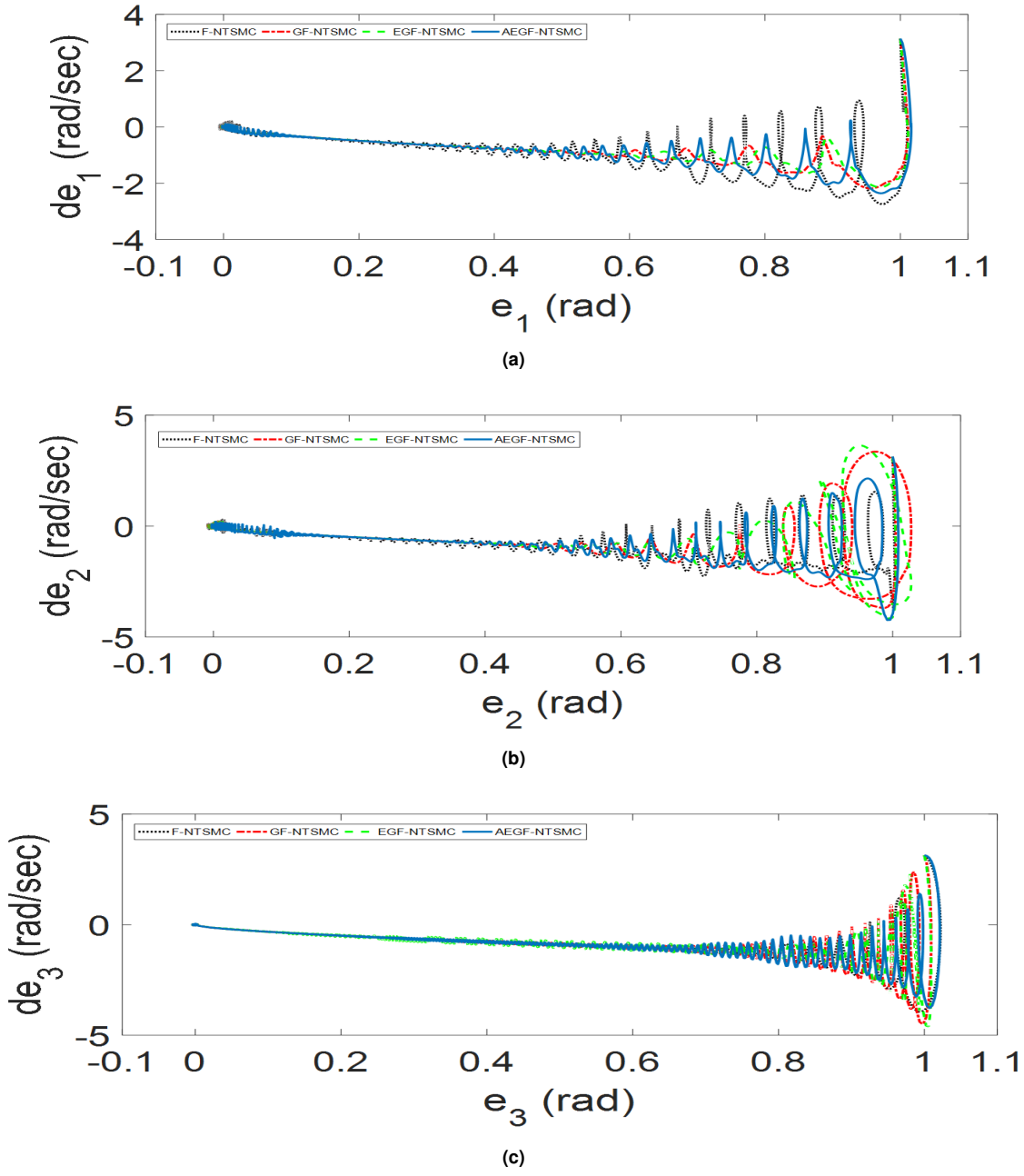

Figure 7. Phase portraits of: (a) Joint 1 (b) Joint 2 (c) Joint 3

only the uncertainty in the length of link 3 is due to the fact that this link is associated with the end-effector for object manipulation. A time-varying external disturbance given in (45) is considered for robustness analysis.

$$\left.\begin{array}{l} q_{d1}(t) = 2 + 0.1(\sin(t) + \sin(2t)) \\ q_{d2}(t) = 2 + 0.1((cos(2t) + cos(3t)) \\ q_{d3}(t) = 1 + 0.1(\sin(3t) + \sin(4t)) \end{array}\right\} \quad (42)$$

$$m_1 = m_{01} + 0.1m_{01},$$

$$m_2 = m_{02} + 0.2m_{02},$$

$$and m_3 = m_{03} + m_{03} \quad (43)$$

$$l_1 = l_{01},\ l_2 = l_{02},\ l_3 = l_{03} + 0.2l_{03} \quad (44)$$

$$\tau_d = \begin{cases} 2\sin(t) + 0.5sin(200\pi) \\ 2\sin(t) + 0.5sin(200\pi) \\ \cos(2t) + 0.5sin(200\pi) \end{cases} \quad (45)$$

As in the first trajectory, results in this second trajectory tracking consists of each joint's response, corresponding

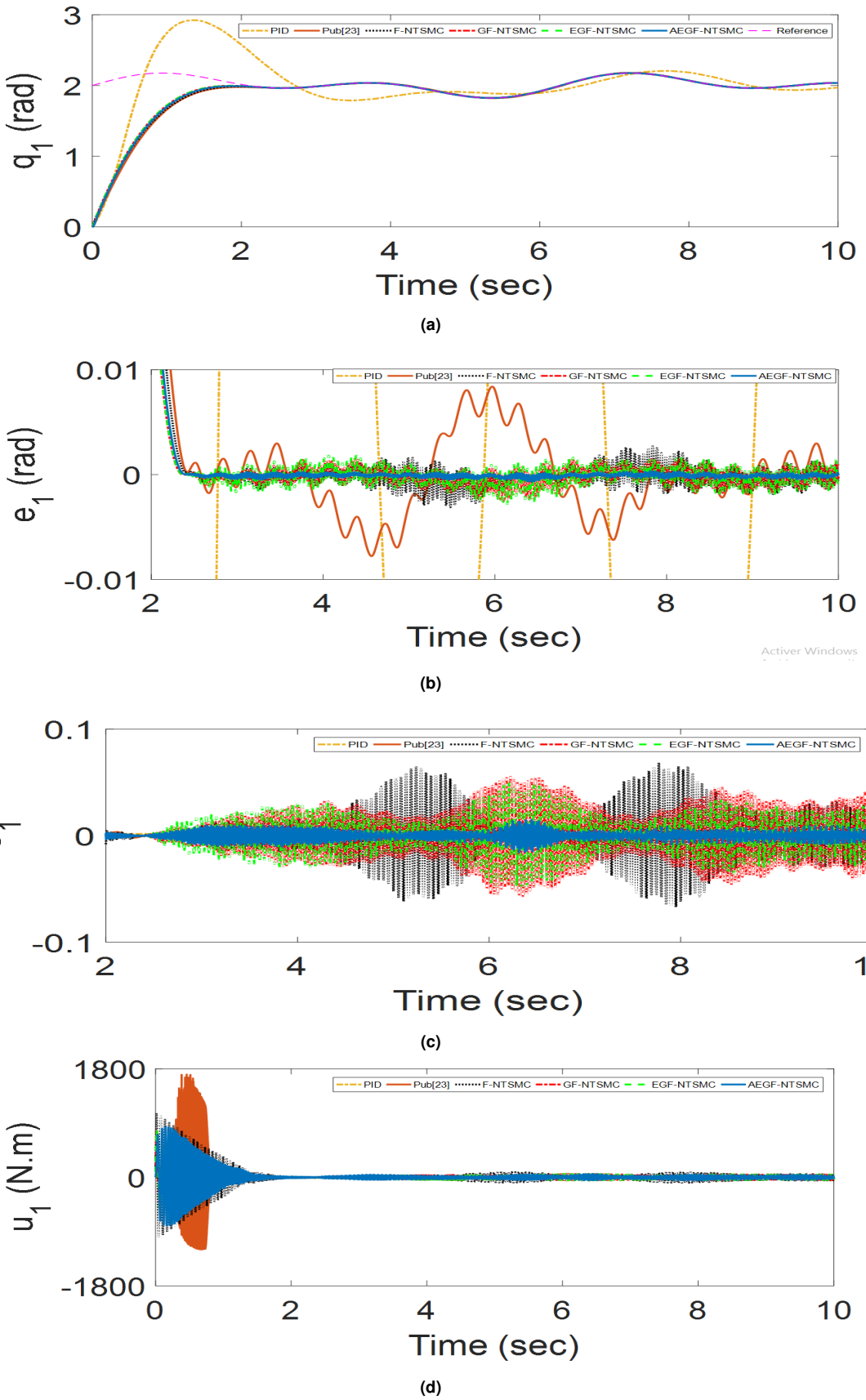

Figure 8. Position tracking performance of joint 1: (a) Joint response (b) Angular error (c) Sliding surface (d) Control input

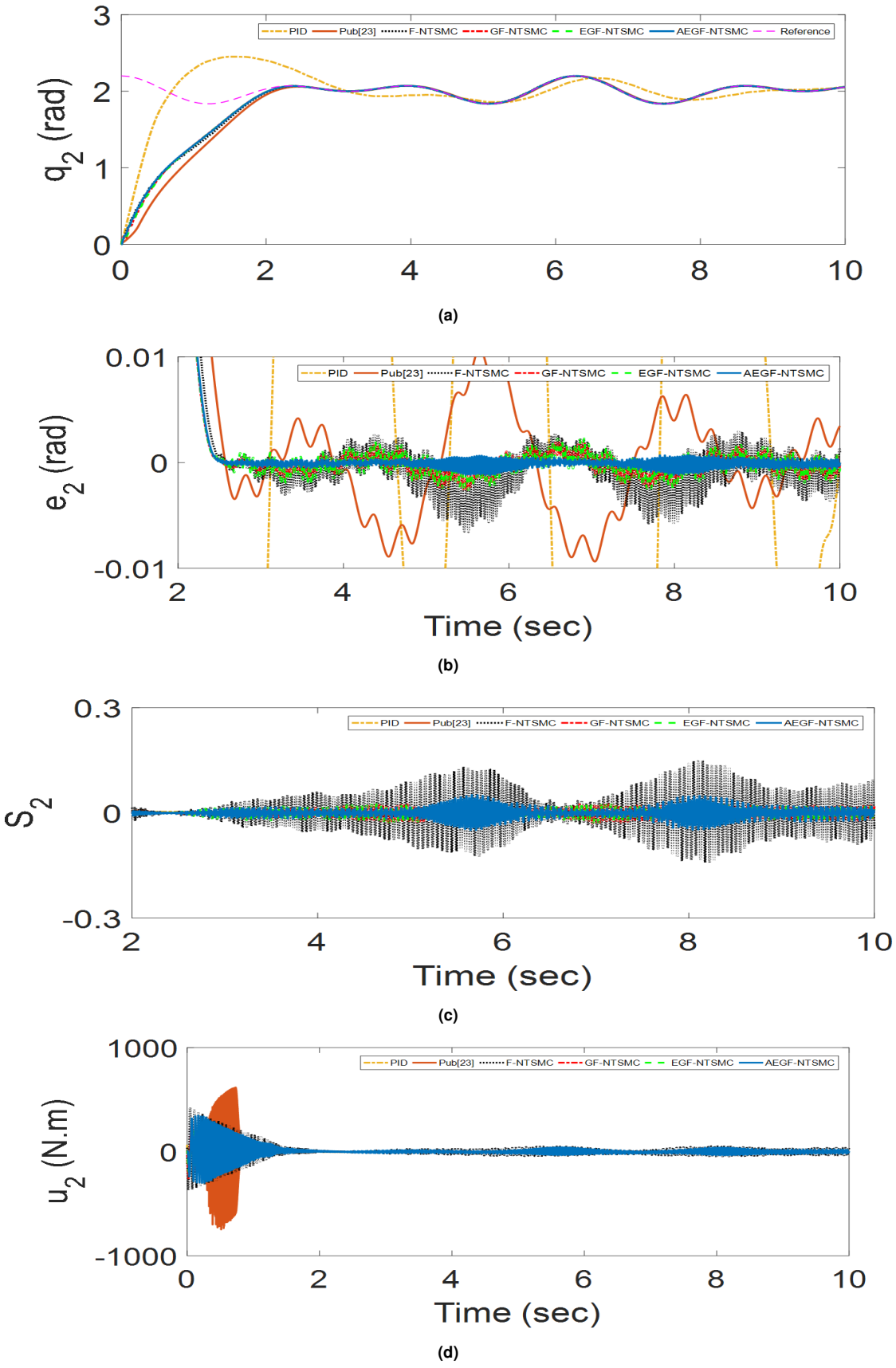

Figure 9. Position tracking performance of joint 2: (a) Joint response (b) Angular error (c) Sliding surface (d) Control input

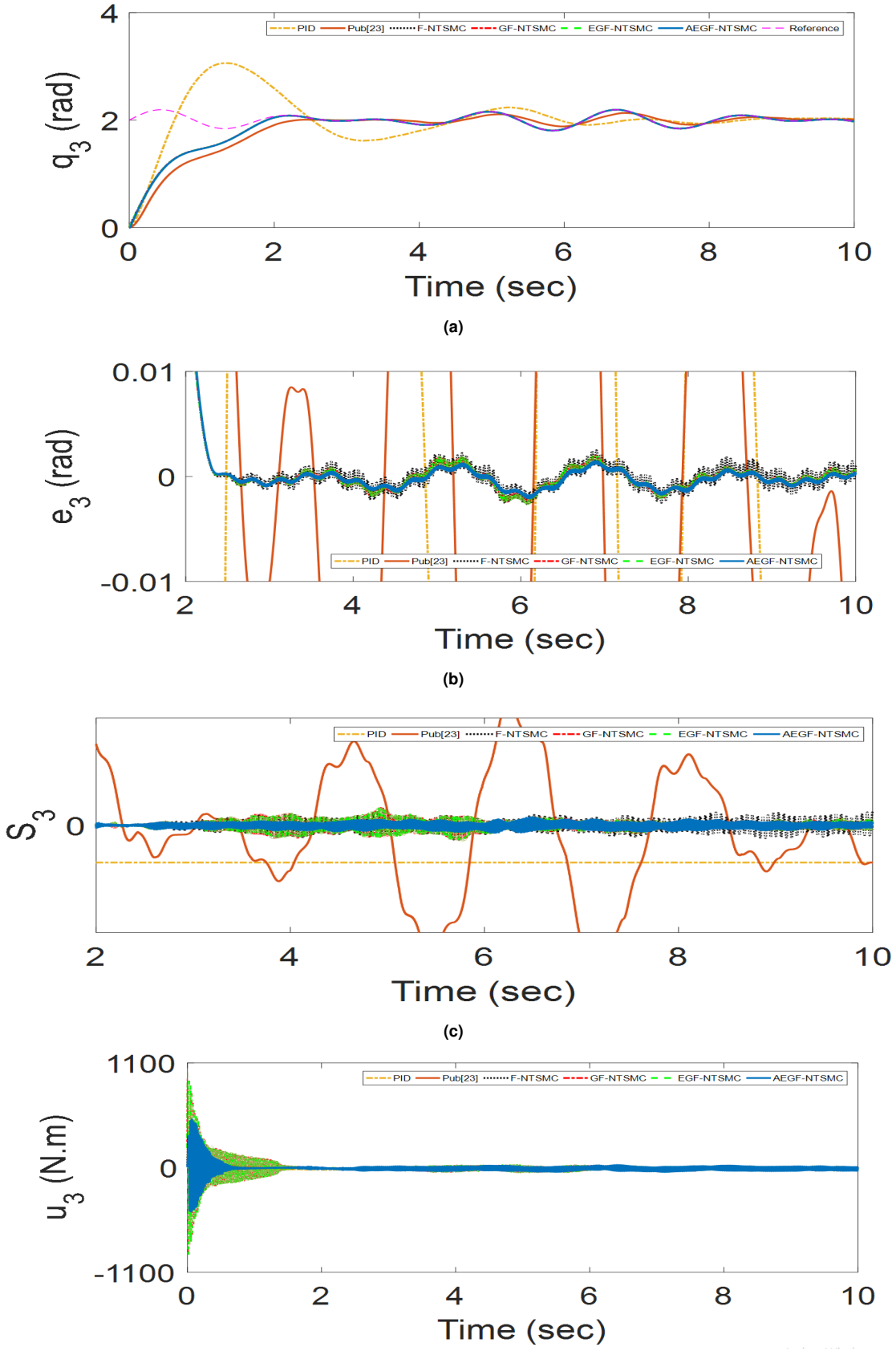

Figure 10. Position tracking performance of joint 3: (a) Joint response (b) Angular error (c) Sliding surface (d) Control input

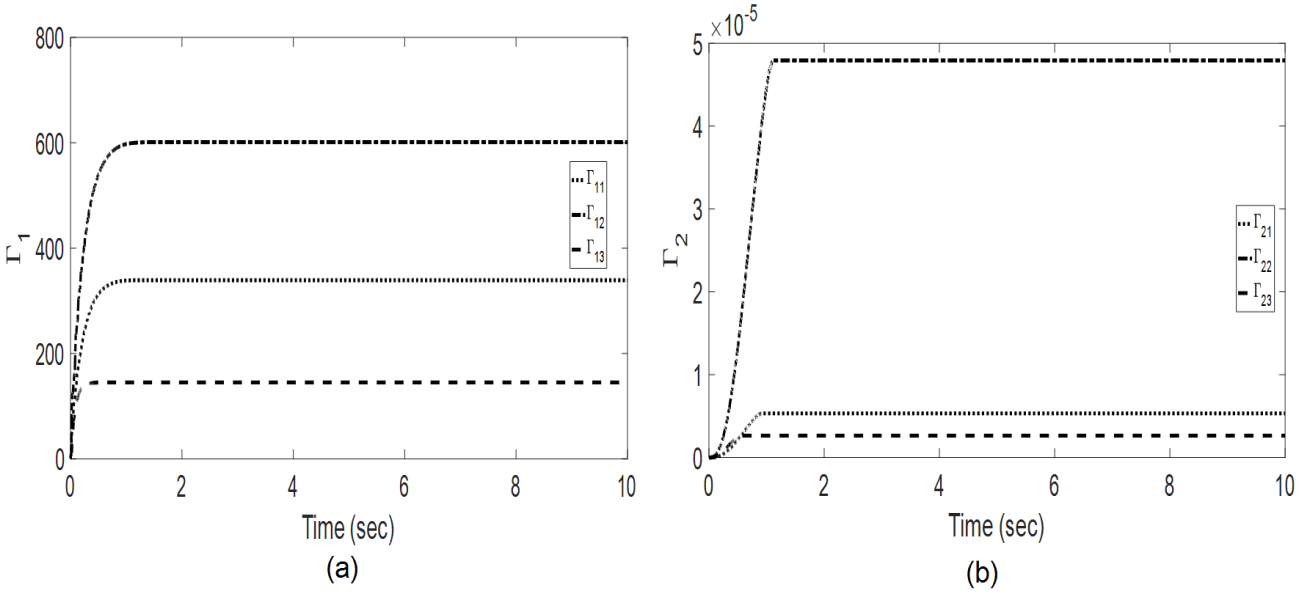

Figure 11. Adaptive gains of the AEGF-NTSMC (a) Alpha (b) Beta

error profile, sliding surface and control signal as illustrated in Fig 8, 9 and 10 in case of joint 1, joint 2 and joint 3 respectively. The tracking performance under parametric variations and external disturbances (42-44) dictates that the desired trajectory is tracked adequately. We can observe that all joints converge to the desired trajectories (within 2 sec). Moreover, all error values tend to zero after a transient time due to errors in the initial conditions. One can observe that the control signals are affected by the disturbances added to the control law. However, this does not affect the system response. The time responses of the sliding surfaces confirm the fast convergence of the system dynamics. The system states reach the sliding manifold in finite-time and then they converge to zero along the pre-described surface. Moreover, the controller AEGF-NTSMC demonstrated fast convergence compared to F-NTSMC, GF-NTSMC and EGF-NTSMC. From the angular position errors, one can observe the greater precision of the AEGF-NTSMC in the presence of uncertainties and disturbances (i.e. maximal errors for joints are $|e_{max1}| \leq 0.00067\ rad$, $|e_{max2}| \leq 0.0012\ rad$, $|e_{max3}| \leq 0.0021\ rad$) compared with EGF-NTSMC where the maximal errors for joints are $|e_{max1}| \leq 0.0026\ rad$, $|e_{max2}| \leq 0.0012\ rad$, $|e_{max3}| \leq 0.0026\ rad$. Finally, it is concluded that the AEGF-NTSMC offers superior performance, such as high tracking precision, fast response, singularity avoidance and strong robustness to external disturbances and modelling uncertainties as evidenced by the desired trajectories demonstrating above-mentioned error profiles. Fig. 11 presents adaptive gains of AEGF-NTSMC. The estimated parameters adaptively increase based on the adaptive laws. The convergence of the estimated parameters indicates that the adaptive mechanism continues to perform adequately and the sliding mode is reached. The positive functions Γ_1 and Γ_2 are obtained by integrating equation (30), which presents the time derivatives of Γ_1 and Γ_2. Integration of (30) yields monotonic functions as confirmed in the simulation results (Fig. 6 and Fig 11). Fig. 12 shows phase portraits of different joints confirming the convergence of the system.

The effectiveness of the proposed AEGF-NTSMC in comparison to other variants of NTSMC is demonstrated considering performance indices ISE and IAE. With a final time of $t_f = 50\ Sec$, the initial time t_0 for ISE and IAE is 2 Sec and 0 Sec respectively. The simulation time is 50 Sec. The performance indices are obtained for the trajectory expressed in (45) in the presence of the disturbances (43-44). The results obtained are given in Tables 7-8.

We can conclude from the numerical results that AEGF-NTSMC has offered best performance compared with the other controllers. Compared to F-NTSMC, ISE and IAE have been improved by 234.99% and 175.24% respectively. It can also be noticed that GF-NTSMC and EGF-NTSMC offer very close performance. However, better results are obtained in case of NTSMC-based GWO compared with the classical one.

Conclusion

In this paper, four robust control methods F-NTSMC, GF-NTSMC, EGF-NTSMC and AEGF-NTSMC have been proposed and applied to a 3-DOF robotic manipulator. AEGF-NTSMC controller was based on TDE method while the optimization has been performed through an emerging meta-heuristic method GWO. An extended GWO (EGWO)

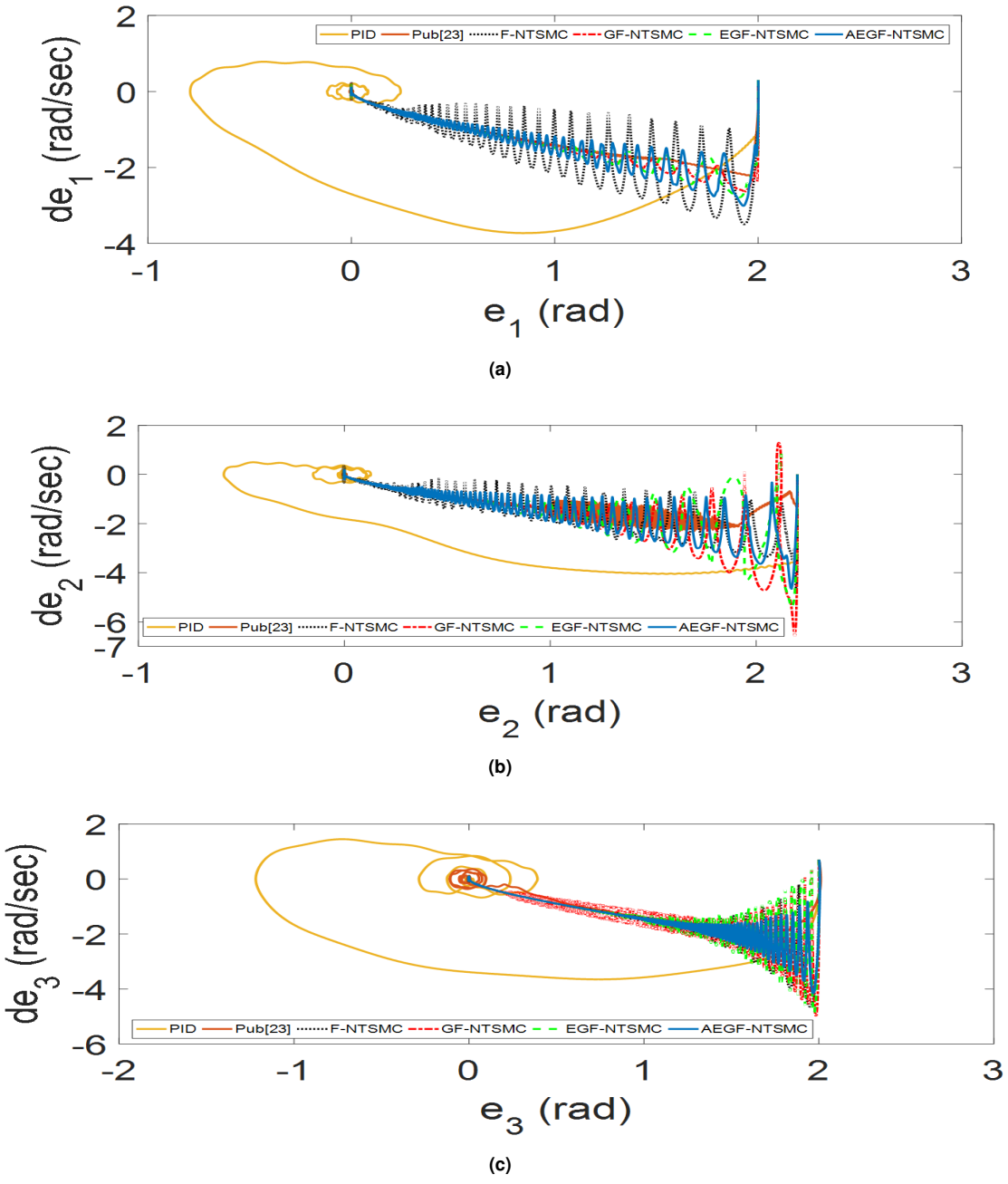

Figure 12. Phase portraits of: (a) Joint 1 (b) Joint 2 (c) Joint 3

Table 7. ISE of AEGF-NTSMC and other NTSMC variants

	F-NTSMC	GF-NTSMC	EGF-NTSMC	AEGF-NTSMC
$\int_{t_0}^{t_f} {e_1}^2 dt$	0.1248	0.0693	0.0690	**0.0505**
$\int_{t_0}^{t_f} {e_2}^2 dt$	0.4455	0.1860	0.1859	**0.1655**
$\int_{t_0}^{t_f} {e_3}^2 dt$	0.0931	0.0834	0.0830	**0.0663**
$left \sum_{i=1}^{3} {e_i}^2$	0.6634	0.3387	0.3379	**0.2823**
%age improvement	100%	195.86%	196.33%	**234.99%**

Table 8. IAE of AEGF-NTSMC and other NTSMC variants

	F-NTSMC	GF-NTSMC	EGF-NTSMC	AEGF-NTSMC
$\int_{t_0}^{t_f} t\|e_1\|dt$	1740.2	1556.5	1556.5	**895.2912**
$\int_{t_0}^{t_f} t\|e_2\|dt$	2.959.9	1753.1	1753	**1384.1**
$\int_{t_0}^{t_f} t\|e_3\|dt$	1773.5	1644.9	1643	**1414.5**
$\sum_{k=1}^{3} t\|e_i\|$	6473.5	4954.6	4952.5	**3693.9**
%age improvement	100%	130.65%	130.71%	**175.24%**

is also proposed in this paper to improve the results of the classical GWO. The main purpose of using GWO and EGWO is to obtain an optimal gain matrix $\bar{M}$, which carries an essential role is TDE-based control methods. Adaptive control proposed in the present work is based on Lyapunov theorem. Simulation results demonstrate that AEGF-NTSMC over-performs in terms of accuracy and finite time convergence. The strong robustness against parametric uncertainties and external disturbances has also been confirmed in AEGF-NSTMC based control law. As per the authors knowledge the present work is a first attempt to synthesize the gain matrix $\bar{M}$ using a metaheuristic method thus avoiding trial and error method. The adaptability of AEGF-NTSMC makes the proposed control technique highly recommended for controlling the robots subjected to high nonlinearities and uncertainties while still demanding the adequate performance.

References

1. J. Iqbal, R. U. Islam, S. Z. Abbas, A. A. Khan, and S. A. Ajwad, "Automating industrial tasks through mechatronic systems–A review of robotics in industrial perspective," Tehnički vjesnik, vol. 23, pp. 917-924, 2016.
2. J. Iqbal, M.I. Ullah, A.A. Khan and M. Irfan, "Towards sophisticated control of robotic manipulators: Experimental study on a pseudo-industrial arm", Strojniški vestnik – Journal of Mechanical Engineering, 61(7-8):465-470, 2015.
3. M. I. Ullah, S.A. Ajwad, M. Irfan and J. Iqbal "Non-linear control law for articulated serial manipulators: Simulation augmented with hardware implementation", Elektronika Ir Elektrotechnika, 22(1): 3-7, 2016.
4. S. A. Ajwad, J. Iqbal, M. I. Ullah, and A. Mehmood, "A systematic review of current and emergent manipulator control approaches," Frontiers of Mechanical Engineering, vol. 10, pp. 198-210, 2015.
5. U. Iqbal, A. Samad, Z. Nissa, and J. Iqbal, "Embedded control system for AUTAREP-a novel autonomous articulated robotic educational platform," Tehnicki Vjesnik-Technical Gazette, vol. 21, pp. 1255-1261, 2014.
6. S. A. Ajwad, U. Iqbal, and J. Iqbal, "Hardware realization and PID control of multi-degree of freedom articulated robotic arm," Mehran University Research Journal of Engineering and Technology, vol. 34, pp. 1-12, 2015.
7. M. Wasim, M. Ullah, and J. Iqbal, "Gain-scheduled proportional integral derivative control of taxi model of unmanned aerial vehicles," Revue Roumaine Sci. Techn.-Serie Electrotechn. Energetique, vol. 64, pp. 75-80, 2019.
8. W. Alam, A. Mehmood, K. Ali, U. Javaid, S. Alharbi, and J. Iqbal, "Nonlinear control of a flexible joint robotic manipulator with experimental validation," Strojniški vestnik-Journal of Mechanical Engineering, vol. 64, pp. 47-55, 2018.
9. Z. S. Awan, K. Ali, J. Iqbal, and A. Mehmood, "Adaptive backstepping based sensor and actuator fault tolerant control of a manipulator," Journal of Electrical Engineering and Technology, vol. 14, pp. 2497-2504, 2019.
10. S. A. Ajwad, J. Iqbal, R. U. Islam, A. Alsheikhy, A. Almeshal, and A. Mehmood, "Optimal and robust control of multi DOF robotic manipulator: Design and hardware realization," Cybernetics and Systems, vol. 49, pp. 77-93, 2018.
11. X. Cao, L. Gu, H. Qiu, C. Lai, and Y. Qin, "Continuous nonsingular terminal sliding mode contouring control of manipulator based on time delay estimation," Proceedings of the Institution of Mechanical Engineers, Part I: Journal of Systems and Control Engineering, vol. 231, pp. 836-848, 2017.
12. F. Yan, Y. Wang, F. Ju, B. Chen, and H. Wu, "Adaptive time delay control for cable-driven manipulators using fuzzy logic algorithm," Proceedings of the Institution of Mechanical Engineers, Part I: Journal of Systems and Control Engineering,2020.
13. J. Iqbal, M. Ullah, S. G. Khan, B. Khelifa, and S. Ćuković, "Nonlinear control systems-A brief overview of historical and recent advances," Nonlinear Engineering, vol. 6, pp. 301-312, 2017.
14. Y. Shtessel, C. Edwards, L. Fridman, and A. Levant, Sliding mode control and observation: Springer, 2014.
15. R. ul Islam, J. Iqbal, and Q. Khan, "Design and comparison of two control strategies for multi-DOF articulated robotic arm manipulator," Journal of Control Engineering and Applied Informatics, vol. 16, pp. 28-39, 2014.
16. J. Baek, W. Kwon, and C. Kang, "A new widely and stably adaptive sliding-mode control with nonsingular terminal sliding variable for robot manipulators," IEEE Access, vol. 8, pp. 43443-43454, 2020.

17. M. Jin, J. Lee, P. H. Chang, and C. Choi, "Practical nonsingular terminal sliding-mode control of robot manipulators for high-accuracy tracking control," IEEE Transactions on Industrial Electronics, vol. 56, pp. 3593-3601, 2009.
18. Z. Ma and G. Sun, "Dual terminal sliding mode control design for rigid robotic manipulator," Journal of the Franklin Institute, vol. 355, pp. 9127-9149, 2018.
19. Y. Feng, X. Yu, and Z. Man, "Non-singular terminal sliding mode control of rigid manipulators," Automatica, vol. 38, pp. 2159-2167, 2002.
20. A. Rezoug, B. Tondu, M. Hamerlain, and M. Tadjine, "RBFNN-HOMS nonsingular terminal sliding control of n-DOF robotic manipulator," Journal of Control Engineering and Applied Informatics, vol. 18, pp. 52-62, 2016.
21. W. Alam, S. Ahmad, A. Mehmood, and J. Iqbal, "Robust sliding mode control for flexible joint robotic manipulator via disturbance observer," Interdisciplinary Description of Complex Systems, vol. 17, pp. 85-97, 2019.
22. Y. Wang, S. Li, D. Wang, F. Ju, B. Chen, and H. Wu, "Adaptive time-delay control for cable-driven manipulators with enhanced nonsingular fast terminal sliding mode," IEEE Transactions on Industrial Electronics,68(3), 2356-2367, 2020.
23. Y. Wang, L. Gu, B. Chen, and H. Wu, "A new discrete time delay control of hydraulic manipulators," Proceedings of the Institution of Mechanical Engineers, Part I: Journal of Systems and Control Engineering, vol. 231, pp. 168-177, 2017.
24. Y. Wang, S. Jiang, B. Chen, and H. Wu, "A new continuous fractional-order nonsingular terminal sliding mode control for cable-driven manipulators," Advances in Engineering Software, vol. 119, pp. 21-29, 2018.
25. M. Boukattaya, N. Mezghani, and T. Damak, "Adaptive nonsingular fast terminal sliding-mode control for the tracking problem of uncertain dynamical systems," ISA Transactions, vol. 77, pp. 1-19, 2018.
26. C. Yang, F. Yao, M. Zhang, Z. Zhang, Z. Wu, and P. Dan, "Adaptive sliding mode PID control for underwater manipulator based on Legendre polynomial function approximation and its experimental evaluation," Applied Sciences, vol. 10, p. 1728, 2020.
27. W. M. Elawady, Y. Bouteraa, and A. Elmogy, "An adaptive second order sliding mode inverse kinematics approach for serial kinematic chain robot manipulators," Robotics, vol. 9, p. 4, 2020.
28. H. Komijani, M. Masoumnezhad, M. M. Zanjireh, and M. Mir, "Robust hybrid fractional order proportional derivative sliding mode controller for robot manipulator based on extended grey wolf optimizer," Robotica, vol. 38, pp. 605-616, 2020.
29. K. Baizid, S. Ćuković, J. Iqbal, A. Yousnadj, R. Chellali, A. Meddahi, G. Devedžić, and I. Ghionea, "IRoSim: Industrial Robotics Simulation design planning and optimization platform based on CAD and knowledgeware technologies," Robotics and Computer-Integrated Manufacturing, vol. 42, pp. 121-134, 2016.
30. K. Baizid, A. Yousnadj, A. Meddahi, R. Chellali, and J. Iqbal, "Time scheduling and optimization of industrial robotized tasks based on genetic algorithms," Robotics and Computer-Integrated Manufacturing, vol. 34, pp. 140-150, 2015.
31. S. Mirjalili, S. M. Mirjalili, and A. Lewis, "Grey wolf optimizer," Advances in Engineering Software, vol. 69, pp. 46-61, 2014.
32. H. Abderazek, A. R. Yildiz, and S. Mirjalili, "Comparison of recent optimization algorithms for design optimization of a cam-follower mechanism," Knowledge-Based Systems, vol. 191, p. Article 105237, 2020.
33. Patre, B. M., et al. Disturbance estimator based non-singular fast fuzzy terminal sliding mode control of an autonomous underwater vehicle. Ocean Engineering, 2018, 159: 372-387.
34. L. Chaib, A. Choucha, and S. Arif, "Optimal design and tuning of novel fractional order PID power system stabilizer using a new metaheuristic Bat algorithm, "Ain Shams Engineering Journal, vol. 08, pp. 113-125, 2017.
35. Yu, Shuanghe, et al. Continuous finite-time control for robotic manipulators with terminal sliding mode. Automatica, 2005, 41.11: 1957-1964.
36. P. Ghaf-Ghanbari, M. Mazare and M. Taghizadeh, "Active fault-tolerant control of a schonflies parallel manipulator based on time delay estimation", Robotica, vol. 39, pp. 1518–1535, 2021.
37. W. Yuqiang, Y. Xinghuo and Z. Man, "Terminal sliding mode control design for uncertain dynamic systems", Systems and Control Letters, vol. 34, pp. 281–287, 1998.
38. H. Sai, Z. Xu, Y. Li et al., Adaptive nonsingular fast terminal sliding mode impedance, International Journal of Precision Engineering and Manufacturing, vol. 22, pp. 1947–1961, 2021.
39. M. Zhihong, A.P. Paplinski and H. R. Wu, A robust MIMO terminal sliding mode control scheme for rigid robotic manipulators. IEEE Transactions on Automatic Control, vol. 39, pp. 2464–2469, 1994.
40. L. Yang and J. Yang, Nonsingular fast terminal sliding mode control for nonlinear dynamical systems. International Journal of Robust and Nonlinear Control, vol. 21, pp. 1865–1879, 2021.

Appendix

proof of eq. 13

Time derivative of (8) is given as

$$\dot{S} = \ddot{e} + k_1 \frac{q}{p} e^{q/p-1} \dot{e} = \ddot{q}_d - \ddot{q} + k_1 \gamma^{-1} e^{1-\gamma} \dot{e}$$

From (3) we can write $\dot{S} = 0$ as

$$\ddot{q}_d - (u - \varepsilon) + k_1 \gamma^{-1} e^{1-\gamma} \dot{e} = 0$$

Then

$$u = k_1 \gamma^{-1} e^{1-\gamma} \dot{e} + K_w sign\,(S)$$

The mismatched modelling ε has been cancelled by the compensation term $-K_w sign\,(S)$. Replacing u in (7), we

obtain the control law given in (13).

Proof of eq. 14

Time derivative of (9) is given by

$$\dot{S} = \dot{e} + k^{-1}\gamma\dot{e}^{\gamma-1}\ddot{e}$$

From (3), we can write $\dot{S} = 0$ as

$$\dot{e} + \varphi(\dot{e})(\ddot{q}_d - u + \varepsilon) = 0$$

with $\varphi(\dot{e}) = k_1^{-1}\gamma\dot{e}^{\gamma-1}$

Then,

$$u = \ddot{q}_d + k_1\gamma^{-1}\dot{e}^{2-\gamma} + K_w sign(S)$$

The mismatched modelling ε has been cancelled by the compensation term $-K_w sign(S)$. Replacing u in (7), we obtain the control law given in (14).